LUND UNIVERSITY

Remote nocturnal bird classification by spectroscopy in extended wavelength ranges

Lundin, Patrik; Samuelsson, Per; Svanberg, Sune; Runemark, Anna; Åkesson, Susanne; Brydegaard, Mikkel

Link to publication

LUND UNIVERSITY

PO Box 117
221 00 Lund
+46 46-222 00 00

Remote nocturnal bird classification by spectroscopy in extended wavelength ranges

Patrik Lundin,[1,*] Per Samuelsson,[1] Sune Svanberg,[1] Anna Runemark,[2] Susanne Åkesson,[2] and Mikkel Brydegaard[1]

[1]Atomic Physics Division, Lund University, P.O. Box 118, SE-221 00 Lund, Sweden

[2]Animal Ecology Division, Lund University, Sölvegatan 37, SE-223 62 Lund, Sweden

*Corresponding author: patrik.lundin@fysik.lth.se

We present optical methods at a wide range of wavelengths for remote classification of birds. The proposed methods include eye-safe fluorescence and depolarization lidar techniques, passive scattering spectroscopy, and infrared (IR) spectroscopy. In this paper we refine our previously presented method of remotely classifying birds with the help of laser-induced β-keratin fluorescence. Phenomena of excitation quenching are studied in the laboratory and are theoretically discussed in detail. It is shown how the ordered microstructures in bird feathers induce structural "colors" in the IR region with wavelengths of around 3–$6\,\mu m$. We show that transmittance in this region depends on the angle of incidence of the transmitted light in a species-specific way and that the transmittance exhibits a close correlation to the spatial periodicity in the arrangement of the feather barbules. We present a method by which the microstructure of feathers can be monitored in a remote fashion by utilization of thermal radiation and the wing beating of the bird.   © 2011 Optical Society of America

OCIS codes: 170.1420, 280.3640, 300.2530, 300.6340, 280.4991.

1. Introduction

Migratory birds, which are highly adapted to manage long flights, cross seas and deserts on their long-distance migrations [1–3]. A great majority of songbirds, although most birds are diurnal, migrate at night [4,5]. During the night they will meet less turbulent wind conditions [6], lower predation rates [7], and they have the possibility to use the daytime for foraging [1,2]. A large proportion of migration also occurs at high altitudes ($>500\,m$) [4]. Because our own perception and classification of birds is based primarily on visual information, studies of nocturnal bird migration are challenging.

There are a number of migration phenomena into which we cannot get insights from the currently applied monitoring techniques. Techniques that enable identification of individual species during these conditions would let biologists address questions regarding, e.g., the timing of migration and flight directions in relation to winds and topography. Comparative studies of species composition between time, sites, and years could be performed, and migration routes of individual species could be monitored. Insight into flight patterns of different species is crucial for the understanding of how wing morphology and physiological adaptations affect decisions on strategies and timing of migration. Detailed analyses of the aerodynamics of bird flight have been extensively pursued using advanced laser methods in a wind tunnel setting; see, e.g., [8]. Knowledge of migration routes and timing of the migration of individual species would also improve our understanding of how and when bird-borne diseases such as avian flu, avian malaria, and tick-borne diseases

are expected to be spread, as well as how seeds will be dispersed [3,4,9].

In addition to identifying new species, automatic monitoring techniques not requiring continuous surveillance from field assistants would allow for more efficient studies during daytime and for species migrating at high altitudes. Scattering spectroscopy of a well-defined section of the sky would allow for a more quantitative evaluation with time-resolved data on the number of passing birds. Such an approach could be a good complement to existing manual observation techniques and enable biologists to address questions such as how densities of different species vary during the day and with the ambient conditions. In addition to species identification, classification of sexes, age classes, and ultimately estimation of the condition of individual birds, often reflected in the plumage, would be desirable.

The undoubtedly most traditional way to study birds and bird migration is visual observation with the aid of a pair of binoculars or a telescope, where the light from the Sun is used as light source and the bird can be identified based on appearance and plumage characteristics. The size, shape, and reflectance spectrum (color) of the bird, filtered through the human visual system, provide information about position, flight direction and species of the bird. As long as the light level is high enough and the distance short enough, this approach is very powerful. However, during the night and at longer distances, other approaches are needed.

In the discipline of remote sensing, information is retrieved from far distances. Typically, the methods rely on several regions of the electromagnetic spectrum, e.g., radio frequency (RF), infrared (IR), visible (VIS), and ultraviolet (UV) to transfer the information. Both active backscattering geometries, passive scattering, obscuration, and thermal emission schemes exist. Previously, a number of such methods have been applied to study the nocturnal migration of birds. Tracking and surveillance radars [10–15], IR cameras [5,15], ceilometers [16,17], and lunar obscuration [18,19] have been applied to study the flight altitudes and flight directions of night migrating birds as well as the number of migrants passing. A couple of studies [20,21] designed to compare different methods have drawn conclusions on the advantages and disadvantages of the tested existing methods. Detection of migrating birds from their calls has also been applied [22,23]. The call counts were significantly correlated with radar counts, but a great deal of the variation in vocalization counts remains unexplained, suggesting that factors other than bird density might influence call counts [22]. Although many migratory songbirds produce different flight calls [23], these calls might not enable identification of all species, and fluctuations in call frequencies due to variables other than bird densities might also confuse estimates from this method. Another way to study migratory routes and behavior of birds is to mount archival light loggers (geolocators) [24] or global positioning system loggers [25] on individual birds. These methods give very informative data but are costly and require capture and recapture of specific individuals. Furthermore, geolocators do not enable detailed studies of the flight behavior of birds relative to topography because the precision of the positional information is limited.

Although existing methods have proven valuable for detection of nocturnal migrants, no method has so far enabled general determination of the species of birds. Information on wing-beat frequency and flight speed from tracking radar makes it possible to group migrants into size groups, because wing-beat frequency and flight speed are similar for birds with similar body sizes [26]. Only a very limited number of species with very characteristic wing-beat frequencies, for example, the common swift *Apus apus*, can be identified by tracking radar [27,28].

While bird coloration in the human visual spectrum and more recently also in the UV region above 300 nm has been studied extensively [29,30], little is known about the plumage properties in the deeper UV, parts of the near-IR (NIR) and mid-IR (MIR), information which might not be relevant for classical bird–bird interaction studies, but might still prove valuable for remote sensing purposes. In the present study we explore three new optical schemes using a broad range of the electromagnetic spectrum, including deep-UV, the full bird-VIS range, NIR, and MIR with the purpose of detection and species identification of night migrating birds. We present the most interesting results from each of the techniques and demonstrate several new opportunities.

2. Materials and Methods

The methods used, including light detection and ranging (lidar), IR studies, and passive reflectance, were partly pursued at Lund University. Both reference measurements and some of the test-range lidar measurements were performed in the university laser laboratories. In addition, field studies were made at a field site at the Kullaberg nature reserve close to Mölle in the southwest of Sweden (N 56° 18′, E 12° 26′). The site is situated on a northwest-pointing peninsula that is a main migration point during the spring migration. Kullaberg is a protected area, and at this location many nocturnal passerine migrants usually pass, arriving from Denmark in the west to southwest after a short sea crossing in the spring and continuing toward breeding areas in the north to northeast. The lidar was strategically positioned near the outermost point of the peninsula, which should give the opportunity to test the technique on any birds passing by. The near-coastal site would enable us to test the lidar technique on coastal birds and locally foraging swallows and martins. For an overview of the field site, see Fig. 1. The work was performed with general ethical permits (nos. M172-06 and M204-06).
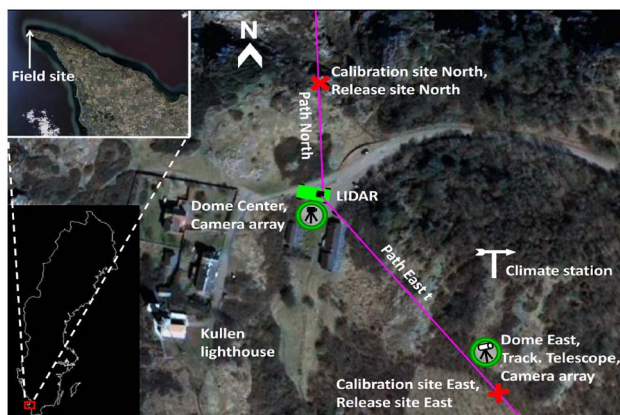
Fig. 1. (Color online) Photographic setup overview of the field site at Kullaberg and its location in Sweden. The site has the coordinates N 56° 18′, E 12° 26′. Shown are the locations of the lidar equipment, the center dome in which the IR cameras were installed, the east dome with the passive telescope, and a weather station. Also shown are two directions in which different lidar measurements were performed.

A. Elastic and Inelastic Reference Measurements at Multiple Excitation Wavelengths

To understand what phenomena to expect in long-range experiments during lidar measurements in the field, effects of, e.g., excitation quenching were studied in detail in the laboratory. The spectral absorption properties of β-keratin are very important, e.g., when choosing the laser source for fluorescence studies. The reflectance and fluorescence at different excitation wavelengths were therefore studied in the following way: a number of museum samples of different bird species containing a diversity of pigments including eumelanin, pheomelanin, various carotenoids, as well as exhibiting structural colors were analyzed using a combined fluoresceins similar to that presented in [31]; modified with an extension further down in the UV and without a GG420 longpass filter. Moreover, the sensor now also included LEDs with emission at 250 and 300 nm (Roithner Laser, UVTOP250 and UVTOP300). Reflectances for the plumage of the sample birds were obtained from 240 to 740 nm.

All observed reflectance spectra were naturally limited by the reflectance of pure β-keratin (white belly of an adult herring gull, *Larus argentatus*). The observed reflectance of pure β-keratin plumage can accurately be described by a (biased Gompertz) function of the form presented in Eq. (1):

$$R_{\text{keratin}}(\lambda) = A \cdot \exp\left(-\exp\left(\frac{\lambda - \lambda_0}{d}\right)\right) + S, \quad (1)$$

where R is the reflectance; A is a value between zero and one (minus S), in our case 68%; λ is the wavelength valid between 240 and 740 nm; λ_0 is the rise position equal to 365 nm; d is a measure of the steepness, in this case with the value 63 nm; and S is the specular reflection of roughly 4%.

The value of S greatly depends on the illumination and observation angles as well as the orientation of the feather barbules. A represents the reflectance at NIR and is a result of the incident photons escaping the field-of-view (FOV) of the detector; thus, it is unrelated to the absorption of β-keratin. A can be expected to vary considerably between different schemes for reflection measurements [32].

To verify the relation between plumage reflectance and fluorescence, presented in Eq. 1 in [31], the relative elastic light as well as fluorescence emissions generated from several excitation wavelengths were evaluated for a variety of pigments. The relation is highly sensitive to errors in the dark spectrum estimation, and any offset will cause the spectrum to tilt slightly in one or the other way. In a case study, we review the golden oriole (*Oriolus oriolus*), pigmented by the carotenoid lutein. The plumage of the bird was excited with three wavelengths, 266, 308, and 355 nm—all important in the lidar community—and the relative fluorescence shapes were measured.

B. Lidar

In a previous paper [31], we introduced laser-induced fluorescence (LIF) lidar to bird studies. We have demonstrated that remote retrieval of chemical information by measuring the chromophore composition from bird fluorescence spectra is a feasible alternative for remote classification of migrating birds. In that paper we discussed in detail various optical phenomena in feathers, such as scattering, absorption, fluorescence, polarization, and interference effects. The phenomena were experimentally studied in laboratory setups; fluorescence and reflectance studies were also performed in a remote fashion, both on museum bird samples and on live European starlings (*Sturnus vulgaris*) in the field [31].

The lidar technique, employing pulsed laser light sent out into the atmosphere, has, ever since the laser's invention, successfully been used in different forms. Examples of standard applications are the mapping of aerosols [33], clouds [34], temperature [35], and wind speed [36] in the atmosphere. Lidar is also used for gas concentration measurements [37–39] and fluorescence studies of, e.g., aerosols [40] and hard targets such as buildings, water compounds, and plants [41,42]. The technique is well documented, and overviews can be found in e.g., [43,44]. Lidar techniques have previously been successfully used for studying the presence and density of birds and diversity of bird species communities in relation to vegetation structure [45–47]. However, with the exception of our feasibility study [31], lidar has so far not been developed for species classification of birds migrating at night. In the present study we have improved the performance of the lidar setup, and we have also performed a detailed investigation of excitation quenching mechanisms and elastic depolarizing ratios.

The Lund University lidar system used has, in general, been extensively described in several
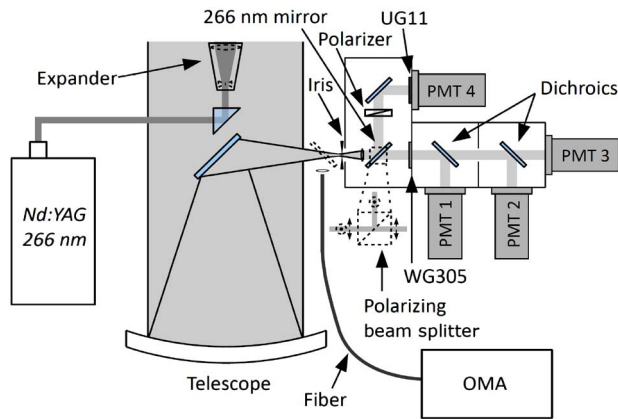
Fig. 2. (Color online) Schematic overview of the fluorescence and polarizing lidar system. The light from the laser is expanded and variably diverged before it is sent out vertically or in other inclinations. The returning light is focused onto the detector system with a 40 cm diameter telescope. Here it is separated into different spectral bands or two polarization directions, or it is sent through a fiber to an OMA.

previous papers (e.g., [48]) and the bird fluorescence lidar variety in an earlier version in [31]. Some important changes have, however, been implemented to improve the bird classification potential, and the most important features of the fluorescence lidar system are therefore presented in Fig. 2. The main improvements of the system are the implementation of one more fluorescence channel and the use of the more suitable, bird eye-safe, excitation wavelength, 266 nm.

Light pulses with a duration of around 4 ns, a wavelength of 266 nm, and pulse energies of around 10 mJ, are obtained by generating the fourth harmonic of a Q-switched Nd:YAG laser (Spectra Physics, Model PRO-200). The light is transmitted into the sky after passing through a Galilean quartz lens expander with the purpose to expand and (variably) set the divergence of the laser beam. The light can be transmitted vertically without any further optics (a tilt-angle quartz window can still be used for weather protection); alternatively, it can be sent out horizontally or with an angle of inclination between $-10°$ to $+55°$ with $0.011°$ angular resolution with the help of a motor-controlled folding mirror (40 cm× 70 cm), also providing the possibility of horizontal angular scanning (360°, 0.0035° resolution).

When light illuminates a bird, part of that light will be reflected, specularly or after several scattering events within the plumage, and part of it will be absorbed, and thus has the possibility to induce fluorescence. A small fraction of the fluorescence and reflected light will return to the lidar and can be focused onto the detecting system by a 40 cm diameter Newtonian telescope. The light passes through a variable aperture, used to control the FOV of the telescope. It is especially important to match the illumination profile and telescope FOV during daytime fluorescence studies when spectrally broad retrieval channels are usually employed. The background

light levels from the scattered sunlight can, under these conditions, heavily compete with the LIF signal, even if the necessary high voltage for the photomultipliers is time gated. Depending on the studies, there are several possible ways to analyze the lidar return. We have in these studies used three different approaches. An image-intensified optical multichannel analyzer (OMA) can record the full spectrum of the light, or a system with a polarizing beam splitter can separate the light into its polarized and depolarized components. The approach mainly used is, however, a four-channel time-resolving detector scheme separating the light into one depolarized elastic laser line channel and three broad wavelength bands, utilizing dichroic beam splitters; see Fig. 2.

1. Optical Multichannel Analyzer Lidar

With the OMA (crossed Czerny–Turner grating spectrometer ORIEL instruments, Model 77400, connected to an image intensified and down to 10 ns time gateable charge-coupled device, ANDOR Technology, Model DH501-25U-01), the full spectrum of the fluorescence from around 300 to 600 nm can be obtained (the range is limited by the second-order diffraction). However, the β-keratin fluorescence intensity rapidly decreases around 600 nm, and not much light is therefore expected at longer wavelengths. The OMA was employed by letting the light, instead of passing through the iris in Fig. 2, be focused into an optical fiber connected to the spectrometer. Even intensified, the sensitivity of the spectrometer is low compared to that of PMTs, and thus this approach is unfavorable in a single-shot situation, which is to be expected when no tracking is utilized and a bird passes by at migrating speed. The OMA system is however very suitable to perform laboratory studies with museum birds when signal averaging can be utilized. This setup was thus used at a docking position of the mobile laboratory in Lund, where light was transmitted to a rooftop some 80 m away, where museum sample birds were positioned, to record the full spectra of their bellies. The laser beam had a spot size diameter of around 6 cm at this distance, and the return collection efficiency of the fiber-coupled spectrometer was optimized by transmitting the 266 nm laser light, and simultaneous to that, sending continuous light from a high-pressure Hg(Xe) arc discharge lamp (Newport, Model 71226) backward through the collecting fiber and overlapping the corresponding spots. The fiber had a diameter of 1 mm, which, together with the focal length of the telescope of 1 m, gives a rough estimate of its collection angle of 1 mrad, equal to a spot size of 8 cm at a distance of 80 m—thus reasonably well matched to the spot size of the laser beam. The fiber was then moved to the spectrometer, and spectra were recorded and averaged for 250 shots for each bird.

2. Multiphotomultiplier Fluorescence Lidar

With four photomultiplier tubes (PMTs) and a system with long-pass filters and dichroic beam splitters, as described in Fig. 2, the returning light can be separated into the depolarized elastic component at 266 nm (separated with a 266 nm HR laser line mirror, VM-TIM UVFS HR > 99.5% at 266 nm, passing through a polarizing cube beam splitter and a UG11 short-pass filter, and recorded with a PMT Model 4816QA/234, Products for Research, Inc.) and three fluorescence bands (split with "UV-Blue" and "Blue-Green" dichroic plate beam splitters from Edmund Optics and recorded with PMT Model 9558/81 from Products for Research, Inc., Model RFI/B-217 from Thorn EMI-GENCOM, Inc., and Model 9558/81/265 from Products for Research, Inc., respectively). The light passes a WG305 long-pass filter before reaching the fluorescence detectors. The chosen fluorescence bands were: UV (around 305–410 nm), blue (around 410–515 nm) and green–yellow (around 515–570 nm) ranges, respectively. The signals were filtered with a 125 MHz low-pass filter to avoid undersampling the short (∼4 ns) bird returns, recorded with a high-speed oscilloscope (Tektronix, Model TDS 544A, maximum 1 GS/s), and stored in a computer via a GPIB connection. The overall collecting speed was 10 Hz, limited by the data readout time, even if the laser repetition rate was 20 Hz. With these relatively broad bands, it is possible to collect enough light in a single shot to get a good signal-to-noise ratio but at the same time get enough spectral discrimination for bird classification. At nighttime, this multi-PMT system was used in a vertical transmitting fashion, sending out light pulses continuously and waiting for bird hits to occur. An automatic software program recorded the lidar returns for later analysis. Using time-gated high-voltage supplies to the PMTs would allow for fluorescence studies even during daytime. This was, however, not achieved during the campaign.

Unexpectedly and unfortunately, the number of birds migrating over the field site was low during the campaign. Therefore, to show an example of a multi-PMT recording of a live bird, such were collected and released at release sites some distance away from the lidar; see Fig. 1. The laser beam was pointed in a direction through which the birds were expected to fly.

3. Depolarization Lidar

The fraction of light illuminated on the bird that is reflected or backscattered with a different polarization direction could possibly provide species specific information. This information can be connected to the previously described laboratory reflectance measurements as the depolarization fraction is highly dependent on the total reflectivity. To explore how the depolarization fraction depends, e.g., on the abundance of pigments in the plumage, and the possible potential of depolarization lidar, measurements were performed remotely on the bellies of eight specimens

of museum bird samples (gray heron, *Ardea cinerea*; herring gull, *Larus argentatus*; chattering lory, *Lorius garrulus*; rook, *Corvus frugilegus*; pallid harrier, *Circus macrourus*; red ibis, *Eudocimus ruber*; barn owl, *Tyto alba guttata*; and sparrow-hawk, *Accipiter nisus*) at a distance of 85 m.

UV light was sent out from the laser, and the 1 mrad divergence resulted in an illumination spot just under 10 cm in diameter on the belly of the birds. The returning light was split into its depolarized and copolarized parts and detected with two separate PMTs. When depolarization studies are performed, the 266 nm HR mirror is switched to a polarizing cube beam splitter (VM-TIM, $R_{II} > 99\%$, $T_\perp > 90\%$), separating the light into a depolarized component and one with preserved polarization direction. A specular reflection, where the light has not been multiply scattered inside the plumage of the bird, should keep its polarization status better than the deeper penetrating light that will lose its polarization information to a larger extent. Furthermore, if the excitation light is significantly absorbed by any present pigment, relative to the absorption in the pure β-keratin matrix, this will reduce the depolarized emission and thereby induce differences between species with more or less of such pigments. In the field, depolarization measurements can be performed during daytime without suffering from the high background light-level, because an interference filter can be employed to block all light except for the narrow elastic laser line.

To establish that it is indeed realistic to obtain the depolarization ratio (DPR) from flying birds as well, measurements were also performed on barn swallows in the field at the site at Kullaberg. The birds were flying at distances between 50 to 200 m from the lidar equipment, over the sea, and close to a cliff. To be able to reach the position of the birds, the beam was transmitted horizontally. Because of this transmission geometry, the angle and part on the birds that was illuminated varied heavily upon, e.g., the flight direction. The results can therefore not be directly compared to reference measurements, which are all taken on the bellies of the birds. However, the possibility of measuring the depolarization from a single shot on a flying bird is demonstrated. In a migration study, for which the lidar would be vertically oriented, measuring birds from below, the illumination would most likely be exclusively straight from beneath which would result in a much more consistent angle of illumination.

C. Infrared Imaging

We also present experimental studies in the MIR region and a novel scheme for passive remote classification in MIR. IR imaging has previously been applied to study nocturnal migration [5,15], but so far studies have focused on detection of migrants and little attention has been given to the spectral domain details of thermal emission from birds.

Colors arising from interference effects, rather than solely from pure spectral differential absorption, are commonly present in various objects in nature [49]. The periodic structures in some materials, with dominant spatial frequencies, induce interference effects, transmitting some colors and reflecting others. The presence of structural colors in insects and bird plumage has been extensively studied, and it has been known long since that some colors are produced by dominant spatial frequencies in refractive index variations rather than by differentially absorbing chemical pigments [49,50]. Bluish and greenish structural colors with wavelengths around 400–550 nm have been correlated with spatial frequencies from transmission electron microscopy (TEM) on nanosized arrays, typically containing submicrometer features [49]. Based on the information that bird feather barbules [the secondary branches of the rachis (trunk), considering that a feather is constructed by the main rachis, barbs, barbules, and hamuli] are well ordered with thicknesses in the order of $2 \mu m$, thus about ten times larger than the structures inducing colors in the blue-green region, one might expect additional structural signatures in the MIR at wavelengths around $4 \mu m$. Studies in the two atmospheric windows, on either side of a CO_2 absorption band in the $3–5 \mu m$ region could therefore provide valuable information. To our knowledge, no studies of the structural bird "colors" in the MIR–thermal IR range have been performed so far. Here we present a novel MIR-based method capable of remotely retrieving information on the microstructure of the plumage.

Further, structural colors are known to often shift upward and downward in the spectral domain depending on the angle of observation with respect to illumination and the ordered matrix [30]. This can be explained geometrically as the effective distances (or spatial frequencies) depend on the angle of observation. If, e.g., the wings of a bird, constituting a substantial part of the area seen from beneath, are considered, the observer angle of view with respect to some feather structures will depend on the wing cycle phase. Observing (tracking) a bird over a complete wing cycle (preferably several) could then result in, e.g., a periodic shift of the MIR wavelength of maximum transmittance of body heat radiation. The features of such shift over time (amplitude, frequency, and bias) could, provide detailed information about the feather microstructures. The ability to retrieve information on the microscopic level over far distances by spectral analysis of the thermal emission could be thought of as remote microscopy. The information is, however, a statistical spatial average.

The potential for spectroscopy in the IR region was studied on sample feathers in the laboratory. Feathers from the outer (dorsal) side of the wings of seven different museum bird species were fixed in reversal film slide mounts. Each slide mount was then fixed to a rotation stage so that the feather could be rotated around the base trunk. For angles of incidence ranging from −45° to +45° in increments of 5° (zero degrees corresponding to normal incidence), the transmittances of the feathers were measured in the range between 2.5 and $25 \mu m$ using a Fourier transform IR (FTIR) spectrometer (ATI Mattson, Model Infinity AR60). In general, the spectra will change according to all three rotations in space, very similarly to what is encountered in crystallography (see, e.g., [51]). The IR source was located on the ventral side of the feather.

To find a connection between the transmittance properties and the spatial structure of the feathers, a transmission microscope (Brunel Microscopes, Ltd., Model SP80, with an AVT Guppy-503 B/C CMOS camera, 810 nm LED illumination) was used to study the features of a number of feathers.

To further explore the feasibility of using the possible spectral information in the IR region, we consider a realistic case. The high metabolism of the flying bird results in an internal body temperature of around 41 °C and causes thermal radiation to be emitted and filtered through the feathers in the bird plumage, as well as through atmospheric absorption. The radiation can then be detected with IR cameras with different detection bands selected by optical filters, preferably on each side of the CO_2 absorption band at around $4.3 \mu m$. Laboratory measurements show that the relative amount of radiation from the bird in each of these bands will differ depending on the transmittance properties of the plumages of different bird species. The relative contribution to each band in the two atmospheric transmittance windows was simulated for a number of birds based on the results from the laboratory spectrometer measurements. The simulation was done by integrating the product of blackbody emission, transmittance for plumage and atmosphere, the normalized detector responsivity of InSb, and optimal transmittance filters for each band. Further, this was done as a function of incidence angle, as described above, to investigate if different birds show any differences in wing-beat-induced dependence on the transmittance.

D. Passive Scattering Measurements

Telescopes have long since been used within the bird research community, but for enhanced visual observation without automation. We implement a telescope connected to a spectrometer for automatic recording and storage of events of spectral intensity change when birds pass through the FOV of the telescope. The sudden difference in the otherwise semistatic spectrum from the sky is recorded, providing information about the coloration of the bird. The same approach can be implemented in moonlight obscuration (so-called moon watching). A Newtonian telescope with an 8″ aperture and 800 mm focal length (Bresser) mounted on an equatorial motorized stage (Messier Model LXD75 GoTo) was installed in the southeast dome of the location at Kullaberg, as indicated in Fig. 1. Clear view to the horizon was achieved in all directions except toward the east.

In the daytime, the telescope was directed toward the star Polaris; thus, in this mode we always had the Sun roughly perpendicular to the optical axis of the telescope. At nighttime, the moon was tracked using the motorized stage included in the telescope setup. In the focal plane of the telescope, a $1000\,\mu$m diameter UV collection fiber (Edmund Optics) was installed feeding the light to a compact spectrometer (Ocean Optics, USB4000). In the daytime we employed a spectrometer slit width of $25\,\mu$m, yielding 1.5 nm resolution, and at nighttime a $100\,\mu$m slit, yielding 6 nm spectral resolution. Cylindrical lenses and second-order rejection filters were installed on the spectrometers. The light was detected by uncooled CCDs. In the daytime we were able to exploit the dynamical range by sample rates of 50 Hz, while in the moon tracking mode at nighttime, we achieved a 100 Hz sample rate, however, with a lower spectral resolution.

3. Analysis and Results

A. Elastic and Inelastic Reference Measurements at Multiple Excitation Wavelengths

The results of the reflectance measurements for the different bird species are shown in Fig. 3. Of particular interest in laser-based remote sensing of airborne β-keratin are certain laser lines. A 95% light absorption by β-keratin can be expected at 266 nm (quadrupled Nd:YAG radiation found in many lidar systems) and some 85% at 308 nm (XeCl excimer lasers typically used in ozone lidars). Although not very powerful, nitrogen lasers emitting at 337 nm might be used where roughly 75% of the light would be absorbed; however, several bird corneas and lenses start to become transparent at 337 nm, thus this choice could be harmful. The tripled Nd:YAG

line at 355 nm is potentially harmful for most bird vision systems, but could be applied for bats or scenarios with limited species involved. Some 65% absorption can be expected at 355 nm. Continuous wave emitting diode lasers at 375 and 405 nm might be used for small-scale experiments without range resolution with some 50% and 40% energy deposition, respectively. The three last-mentioned choices would, however, largely influence the birds and, further, many of the pigments would not be covered within the fluorescence emission range.

Reflectance at 266 nm is dominated by the specular contribution and is therefore highly dependent on the orientation of the feather structures. Because the reflectance is low, the relative accuracy is poor. Because the reference sensor was originally designed for nonordered samples and because of the cylindrically symmetric geometry [31], the reflectances at the various wavelength regions are difficult to combine. With respect to lidar measurements, this fact suggests that the depolarized elastic part is preferred in terms of normalizing the fluorescence. Within the group of diversely reflecting species, all of the reflectance data at 266 nm were nicely described by a β-distribution with mean of 34 per thousand and variance of 0.3 per thousand. Only a weak correlation between 266 nm and the reflectance at 308 nm of 33% was found, and 40% with 355 nm. Possibly the correlations are higher if the specular reflectance is rejected by observing only the depolarized contribution. The reflectance at 308 nm correlated 75% with the reflectance at 355 nm. Thus, normalizing fluorescence with the elastic signal at this excitation wavelength is slightly less favorable in terms of stability.

The data from the fluorescence measurements are not included here, but the combined case study measurements of reflectance and fluorescence at three excitation wavelengths for the golden oriole are presented in the bottom part of Fig. 3. The dark currents for each spectrum were compensated for so that the part of the spectrum between 550 and 650 nm that is not affected by lutein chromophores remains flat. The ratio spectra (see Eq. 1 in [31]) were scaled to match the elastic ratio for the unpigmented part. The double absorption dip of lutein indicates that greater contrast, between the spectral part affected by the chromophore and the unaffected part, is achieved for the lower excitation wavelength. We further note that the contrast in the 266 nm excited fluorescence ratio is better than that for the relative elastic light. This could be explained by the fact that the light is produced internally in the β-keratin matrix; thus, there is no specular contribution, which typically worsens the contrast in the elastic reflectance case.

A surprising result from the fluorescence measurements was that the gray heron showed even stronger fluorescence intensity in the UV than the unpigmented white herring gull. The same results were found from the lidar OMA measurements (results described in next section) and the bird was therefore
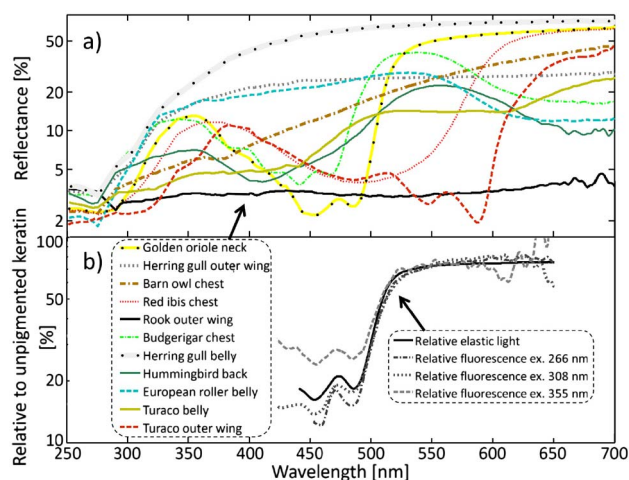

Fig. 3. (Color online) a) Reflectance spectra for different birds at locations specified in the legend. All of the birds are specified elsewhere except for the budgerigar, the hummingbird, and the turaco with Latin names *Melopsittacus undulates*, *Colibri thalassinus*, and *Tauraco erythrolophus*, respectively. b) Fluorescence spectra ratios for the golden oriole. The fluorescence is given relative to unpigmented β-keratin. Excitation at 266, 308, and 355 nm.

investigated in more detail. It was seen that the chest showed spotwise higher reflectance than unpigmented β-keratin in the region 240 nm–340 nm. Consequently, even the fluorescence induced by 266 nm is higher in that region.

B. Lidar

1. Optical Multichannel Analyzer Lidar

The lidar fluorescence returns from six museum bird samples were recorded, and their spectra averaged over 250 shots. The raw spectra of the birds are shown in Fig. 4a). Included in the figure is also the overall spectral transmittance for the bands that were chosen for the multi-PMT setup. The bands are chosen to maximize the classification possibility based on differences in spectra between birds. The natural way to choose the positions of the bands would be to match the visual bands of the birds. In these experiments we have, however, limited ourselves to three fluorescence bands. The positions of these bands are matching reasonably with the visual bands of the birds. The UV band goes from 305 to 410 nm while, as an example, the starling's (*Sturnus vulgaris*) UV band is centered at 362 nm; the blue
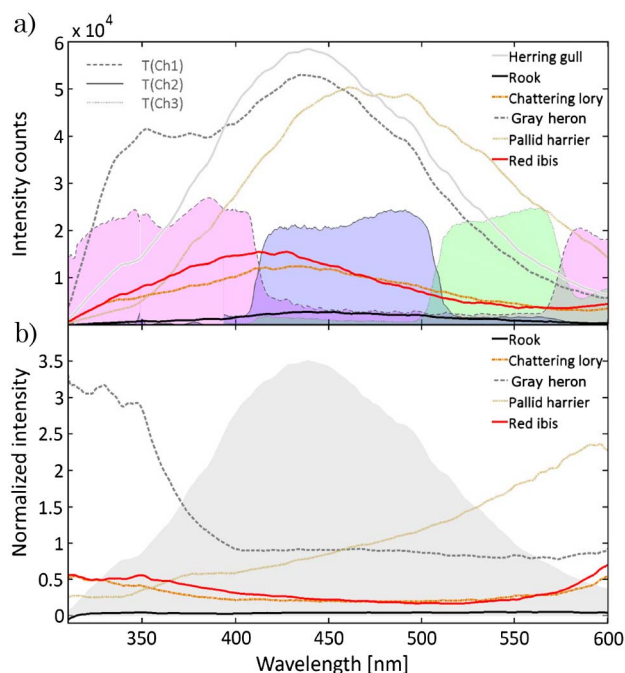

Fig. 4. (Color online) Fluorescence spectra from six birds as remotely obtained by the optical multichannel system. a) The spectra are averaged over 250 shots and smoothed with a 20-channel floating average. Included in the figure is also the overall spectral transmittance in each channel. In these curves are included the transmittance through all optics after the telescope but not the quantum efficiency of the PMTs. What can be noticed is that the UV channel also has some transmittance in the yellow region. However, the lower quantum efficiency of the PMT in this region, in combination with the low emission from β-keratin here, makes the contribution from this region to the total signal small. b) The same spectra divided with the herring gull spectrum.

band is between 410 and 515 nm while the starling's two middle bands are centered at 449 and 504 nm, respectively; the green band is from 515 to 570 nm and the corresponding band of the bird is centered at 563 nm [52]. The white plumage from the herring gull belly was chosen as a reference, due to its general lack of pigments. In order to more clearly reveal differences between the birds, their spectra are divided with the one from the herring gull, as shown in Fig. 4b). From previous studies, [31], we know that the fluorescence color is, in general, well correlated with the reflectance color and the same conclusion can be drawn from Fig. 4. The UV light of the laser induces fluorescence in the β-keratin in the feathers. This actual fluorescence spectrum does not vary much between birds, but when this "white" light is filtered through the plumage, it gets a bird-specific fingerprint through reabsorption. It can be mentioned that the black rook, absorbing much of the fluorescence, shows a very low light level throughout the spectrum. The red ibis and chattering lory, which are both red, show very similar and quite weak fluorescence spectra with a tendency of increased intensity toward the red side of the spectrum. The light-brown pallid harrier belly is also shifted toward the red compared to the herring gull. The increase of its spectrum, however, starts at lower wavelengths, which, combined with our higher visual sensitivity in the green region, makes this bird look brown and not red (what we see is, of course, reflectance, but we here assume that the fluorescence and reflectance are well correlated). The gray heron shows strong signal to the red, but its very strong signal in the UV was especially remarkable.

2. Multiphotomultiplier Fluorescence Lidar

The performance of the multi-PMT setup was determined by pursuing measurements on the same museum sample birds as the ones in the OMA section, but now on a single-shot basis. For each shot, the lidar returns in the four channels were recorded with the oscilloscope and saved through a LabView (National Instruments) interface. The echo return powers were automatically calculated with the help of a scheme that (i) sorts out the files containing bird echoes, (ii) finds the distance in that return at which the bird is considered to be, and (iii) calculates the echo power from the bird in each channel by integrating the signal from the full bird return. The last step is needed because the trigger jitter and the impulse response of the PMTs might differ slightly between channels. The peak-height alone could therefore be misleading or inaccurate. In Fig. 5, the information obtained is presented in an isosurface histogram plot. Here the different birds will end up at different positions in this three-dimensional (3D) color space constructed with the echo power of the three fluorescence channels normalized to the depolarized elastic channel as the axes. The 3D space is divided into 20 × 20 × 20 cubic bins, and, depending on the echo power
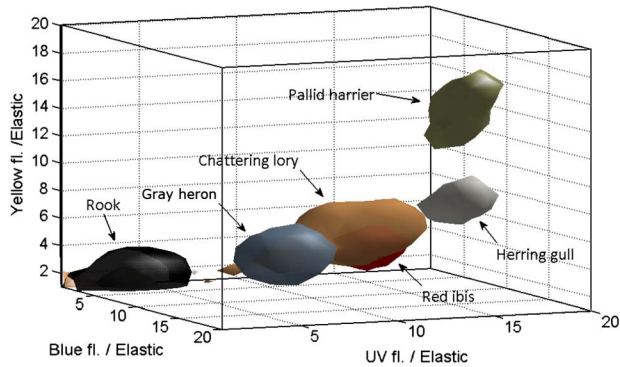
Fig. 5. (Color online) Isosurface 3D histogram plot for the fluorescence return from different birds. Depending on the fluorescence spectrum, different birds gather at different locations in the 3D space made from the three fluorescence channels normalized with the depolarized elastic channel.
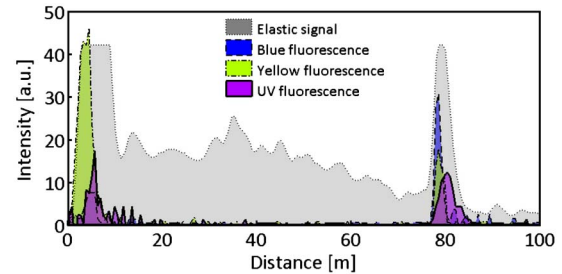

Fig. 6. (Color online) Lidar signals in the depolarized elastic and the three fluorescence channels during a released bird event (for the geometry, see Fig. 1). The bird is a lesser whitethroat released at 23:34, 28 May.

in each channel, every lidar return will end up in one of these cubes, creating a 3D histogram field. The 3D histogram produces a probability distribution. A measurement at a later stage of an unknown species can be indexed in the histogram, and the probability for the unknown sample to belong to a certain species is given by its position in the color space. A surface with a certain confidence level, in the presented case 70%, is drawn in the histogram, meaning that a bird of the corresponding species would, with 70% probability, end up within this surface. The tendency of the echoes from the different birds to cluster at different places in this grid is clear. This implies that there is a potential for remote bird classification. The measurements are performed on one single individual of each species. Some larger spread could be expected if many individuals were included. On the other hand, further improvements of the system, e.g., using four fluorescence bands matching the vision bands of the birds, could compensate for this increased variation.

Fluorescence signals were also recorded of the live released birds, and an example of that is shown in Fig. 6. The example bird is a lesser whitethroat (*Sylvia curruca*), and the data are recorded at a distance of 80 m from the lidar.

3. Depolarization Lidar

The DPR is defined in Eq. (2):

$$\mathrm{DPR} = \frac{I_\perp}{I_\perp + I_{\mathrm{II}}}, \qquad (2)$$

where I_{II} is the copolarized intensity and $I_\perp$ is the depolarized intensity. In our case we have used the integrated echo power, as described in the previous section, as a measure of the return energies. As the two polarizations are recorded with different detectors and in different detector geometries, the signals have to be calibrated in order to get a quantitative axis for the DPR. In these measurements, we have calibrated the system by including a measurement

on a reference polystyrene plate with the well-known DPR. Included is also a measurement on a plate of diffuse aluminum, which should have a low DPR as long as the system does not suffer from interchannel leakage.

The results of the measurements on the museum birds are shown in Table 1. The mean DPRs with standard deviations are shown.

In Fig. 7, examples of lidar returns from a flying barn swallow (*Hirundo rustica*) and the museum gray heron are shown. In this case, the barn swallow was flying at a distance of 150 m. The signals in this specific example are low due to a partial hit. However, the strength in the two polarizations could still be compared. Pure hits on flying barn swallows also occurred with strong resulting signals, however, at closer range.

During the depolarization measurements on the barn swallows, a considerable amount of hits occurred, for which the position along the axis of the laser beam was recorded, as well as the time for the event. Histograms in the time and space of lidar signals can effectively be used to, e.g., map out preferred locations and flying times. This can then be correlated with, e.g., wind data or other conditions of interest. In Fig. 8, example histograms of the distance from the lidar equipment to the birds, and the time of the bird hit, are shown for recordings during the time 17:55 to 18:33 on 25 May 2010. A threshold taking into account the static backscatter light and the range-dependent signal strength was employed to recognize rare events of reflections from birds. This threshold was, in this case, set with quite a margin to make sure that all hits shown in the histogram are from birds and not from, e.g., smaller insects [53], which could also be seen as smaller events.

C. Infrared Imaging

Examples of the IR transmittance spectra of feathers from three museum bird species: a blackbird, *Turdus merula*, the sparrow-hawk, and the pallid harrier at normal incidence are shown in Fig. 9, in addition to the spectral detectivity profiles of three different IR semiconductor detectors, as well as the atmospheric transmittance in the region. The lower transmittances at around 3.0, 6.1, and 6.5 μm in the feather spectra are caused by β-keratin absorption. The peak

Table 1. Remotely Measured DPRs at 266 nm Reflectance for a Gray Heron (*Ardea Cinerea*), Sparrow-Hawk (*Accipiter Nisus*), Red Ibis (*Eudocimus Ruber*), Chattering Lory (*Lorius Garrulus*), Barn Owl (*Tyto Alba Guttata*), Herring Gull (*Larus Argentatus*), Pallid Harrier (*Circus Macrourus*), Styrofoam, and Aluminum

Species	Gray Heron	Sparrow-Hawk	Red Ibis	Chattering Lory	Barn Owl	Herring Gull	Rook	Pallid Harrier	Styrofoam	Aluminum
Mean DPR [-]	0.354	0.332	0.301	0.286	0.270	0.262	0.255	0.255	0.302	0.054
Standard deviation	0.008	0.037	0.017	0.018	0.012	0.009	0.019	0.011	0.007	0.010

at the $5.9\,\mu$m wavelength is due to the Christiansen effect, which occurs when the refractive index of air coincides with that of β-keratin [54]. This occurs on the lower wavelength slope of β-keratin absorption due to the Kramers–Kronig relation. The spectral position of a transmittance peak within the region 4.0 to $5.5\,\mu$m was found to be dependent on both bird species and the angle of incidence of the transmitted light. Plumage iridescence (i.e., the shift of wavelength of peak reflectance—or in this case transmittance—under an altered angle of observation, due to structural interference) has been studied in depth in the optical regime [29], and the result from our measurements shows that an analogous effect exists in the MIR. In the VIS region of the spectrum, iridescence is usually related to thin-film interference caused by sub-micrometer-scale structures inside feather barbules [29]. These are sometimes rather larger in size than the wavelength of peak reflectance, in which case the optical phenomenon is caused by higher order reflectance peaks with the zero-order peak in the NIR [29]. In order to investigate what is causing the observed peak shift in the MIR region, a feather from a herring gull was stretched in total 40% laterally and perpendicular to the trunk (approximately increasing the barb separation in the same way) in 15 steps, and the spectral transmittance was measured at each increment. The results (not presented here) show a shift of peak

transmittance from the 4.2 to $4.5\,\mu$m wavelength. Assuming that barbs or barbules are only rotated or shifted, not deformed in the process, this result shows that the MIR iridescence is not caused within individual barbs/barbules/hamuli but rather by the feather (or the β-keratin–air matrix) as a whole. The barbules, which are organized in a laminar fashion, constitute the majority of the interrogation area, and they also have a thickness that is of the same order of magnitude as the wavelengths.

In [55] it is shown analytically that the intensity of light scattered into a vector k in a medium consisting of quasi-ordered cylindrical fibers suspended in a medium of different refractive index, is proportional to the inverse of the Fourier frequency spectrum of the variation in refractive index along k. This result has been successfully applied in a number of cases to predict the reflectance spectra of feathers [56]. In [56], the variation in refractive index was estimated from the two-dimensional (2D) spatial Fourier spectra of TEM micrographs of cross-sectional slices of barbules. In the present study, we are instead exploiting the fact that the barbules are organized like Venetian blinds, which suggests that even for normally incident light, there is still some photon transport laterally in the feather, and thus the lateral spatial frequency of the barbules can be expected to influence the resulting reflectance spectra and by extension the transmittance spectra of the feathers. The fact that the sizes (or separations) in one of the spatial dimensions are usually well correlated to the sizes in the other two suggests that the spatial lateral frequency should be correlated with the one normal to the surface. In this way, we can expect
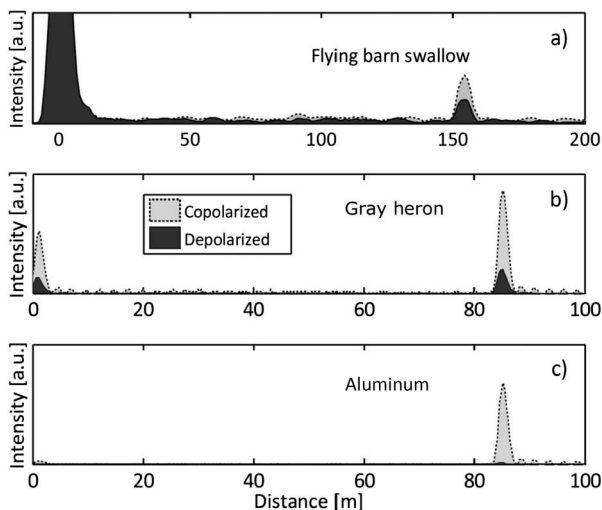

Fig. 7. Lidar returns in a copolarized (dotted curve, light gray) and a depolarized (solid curve, dark gray) channel for a) flying barn swallow, b) museum sample gray heron, and c) aluminum plate.
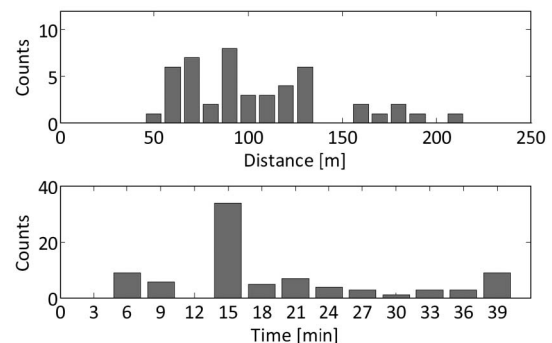

Fig. 8. Histograms over the lidar return distributions in time and space for flying barn swallows recorded during a time span of 38 min. The direction in which the recordings are done is marked "Path North" in Fig. 1.
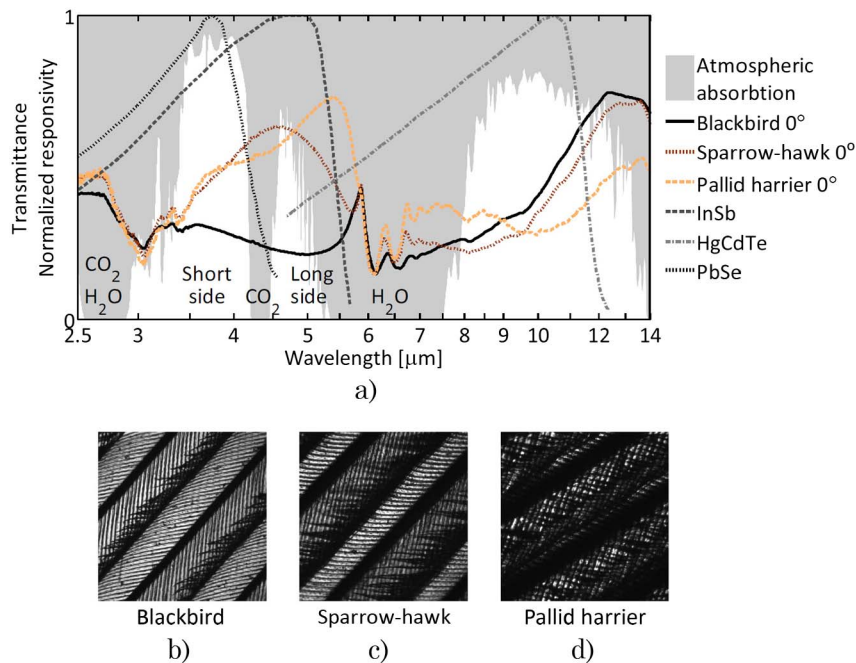
Fig. 9. (Color online) a) Spectral overview of structural MIR effects. The transmittance of three bird feathers at normal incidence shows significantly different spectral features in the wavelength region 3.5–5.5 μm. For demonstration purposes, the feather transmittance spectra have been normalized to the Christiansen peak at 5.9 μm wavelength and the transmittance dip at around 6.1 μm, due to β-keratin absorption. Gray areas denote atmospheric absorption with the primary responsible species indicated. Also shown is the normalized responsivity of three different semiconductor detector materials. Below, sections of the micrographs used for spatial frequency analysis, showing barbules attached to opposite side of the barbs of the same b) blackbird, c) sparrow-hawk, and d) pallid harrier feathers.

that the spectra should be correlated to the measured lateral spatial frequency, even without lateral photon transport.

The spatial frequencies of the distal barbules of a number of sample feathers were estimated by the 2D FFT of light micrographs of the feathers, and the mean barbule periodicities in the plane of the feather surfaces were found as the reciprocal of the spatial frequency peaks (the azimuthal average was used to find the spatial frequency). The resulting inter-
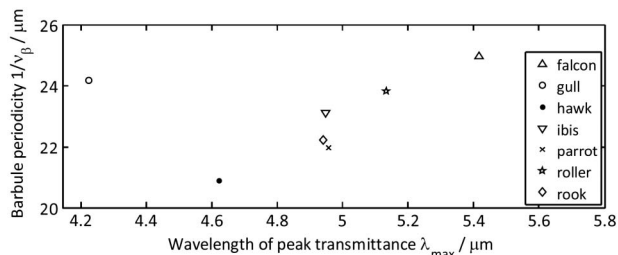

Fig. 10. Correlation between the periodicity of the distal barbule separation and the wavelength of peak transmittance for different bird feathers. It must be stressed that there is a significant uncertainty regarding both the wavelength of peak transmittance as well as barbule periodicity. The keratin absorption bands near 3 and 6 μm, as well as the tail of the Christiansen peak, will affect the transmittance spectrum of keratin, resulting in a shift of the wavelength of maximum transmittance that would result from interference alone. Along the other axis, the measured interbarbule distances depend both on the location on the feather, and can be expected to further deviate for different feathers on the same individual bird.

barbule distances were then correlated to the wavelengths of peak transmittance for normally incident light for each feather, obtained from the Fourier transform spectrometer measurements. The result of this approach is presented in Fig. 10. A subset of six of the seven feathers measured with the microscope (the pallid harrier, the herring gull, the sparrow-hawk, the red ibis, the chattering lory, a European roller, *Coracias garrulus*, and the rook) exhibits a linear relationship between interbarbule spatial periodicity and peak transmittance wavelength with a correlation coefficient equal to 0.96 along one direction and 0.74 along the other (corresponding to directions perpendicular to barbules attached to opposite side of the barbs). This result further reinforces the evidence that the observed MIR interference effects are due to structural features caused by the feather microstructure, and it also suggests a way to remotely retrieve microscopic information from the plumage.

Because the wavelength range with a large variance in the feather spectra falls mostly within the atmospheric window between 3 and 5.5 μm, the ratio between the signals from two spectral bands to either side of the CO_2 absorption band at 4.3 μm would be a candidate for remote classification. Species-dependent time modulation of the signal due to wing-beat patterns introduces another discriminating factor.

The proposed passive method for bird classification utilizes the metabolism of the bird as an IR

source, with an intensity distribution assumed to be that of a blackbody, and the cold sky as background. Spectral emissivity within an atmospheric window is low by definition, and the radiation emitted along the atmospheric path can therefore be neglected. Observations at elevation angles close to vertical will minimize the atmospheric path length and radiance. The choice of wavelength region also means that the resulting atmospheric scattering will be low compared to shorter wavelengths, further increasing the signal-to-noise ratio.

In a simplified model, the detector signal from light transmitted in a spectral band, b, is given by Eq. (3):

$$L_b = \int L(\lambda)\mathsf{T}(\lambda)S_b(\lambda)\mathrm{d}\lambda, \qquad (3)$$

where λ is the wavelength, $L(\lambda)$ is the spectral radiance of the source, $\mathsf{T}(\lambda)$ is the atmospheric transmittance along the path between the source and detector, and $S_b(\lambda)$ is the combined transmittance of the optical filters and normalized detector responsivity. However, reflected radiation from the Earth might contribute substantially to the total detected signal in a practical case. The ratio between the radiance in the atmospheric transmittance bands at the short and long sides of the CO_2 absorption (denoted "Short side" and "Long side" in Fig. 9) depends on the angle of incidence of the transmitted light through the feather, or equivalently, the angle of observation of the bird's wings, given by Eq. (4). This angle-dependent ratio is shown for three different species of birds in Fig. 11:
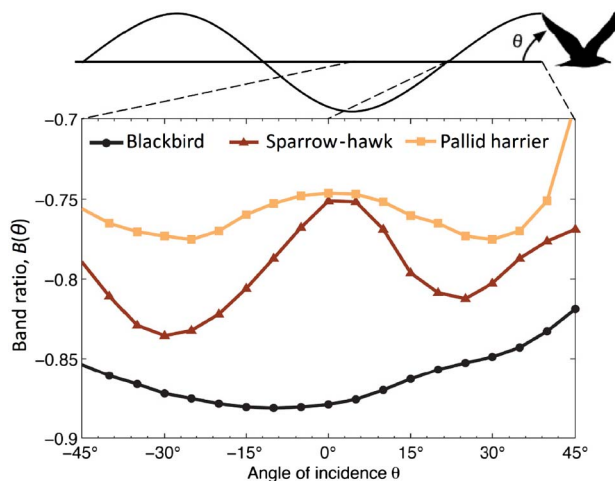

Fig. 11. (Color online) Calculated ratio between long and short (wavelength) spectral bands (relative slope) for blackbird, sparrow-hawk, and pallid harrier feathers. Ideal bandpass filters were used for calculations, defined as having spectral transmittance equal to 1 for wavelengths λ in the interval I, and 0 otherwise, where I was chosen as 2.7 to 4.3 μm for the short-wavelength band, and 4.3 to 5.5 μm for the long-wavelength band, corresponding to the two atmospheric windows on either side of the CO_2 absorption band at around 4.3 μm.

$$B = \frac{L_{\text{long}} - L_{\text{short}}}{L_{\text{long}} + L_{\text{short}}}. \qquad (4)$$

The ratio, B, is calculated from the blackbody spectrum as given by Planck's law with absolute temperature $T = 315\,\text{K}$, detector responsivity of indium antimonide (InSb), and experimental feather transmittance spectra as measured using FTIR for angles of incidence, θ, between $-45°$ and $+45°$, when rotated around the trunk. The results show a distinct difference in shape between the three species—a fact that could hopefully be used in a live situation.

D. Passive Scattering Measurements

On 26 May 2010, 1,592,000 passive sky spectra were collected from 12:54:56 to 19:24:29. The data were loaded into MATLAB software (MathWorks). Darkness was presumed in the range 180 nm–260 nm, and this range constituted to a dark current estimation, which was subtracted from the data. To overview the data, we applied singular value decomposition (SVD). In total, eight significant spectral components were found. After rotation of the coordinate system from the SVD, one component could be associated with the temperature of the spectrometer, changing over the day. This component showed up as a derivative of the Fraunhofer lines and thus implies a shift of the spectrum due to the mechanical deformation internally in the spectrometer. After correcting data for the instrument temperature by rejecting the corresponding component, also the cosine of the true Sun time of the day could be accurately predicted independently of passing clouds. This was done by a simple hyperplane model. The spectral component accounting for the true Sun time showed reciprocal wavelength dependence and can be assumed to correspond to the total air mass in the light path. In principle, we can reject the time component as well and maintain a constant static Sun spectrum over the day. However, the rare events are likely to be influenced by the time of day anyhow, because the birds cannot be considered as spherical particles and because of the interruption of the static geometry.

The total intensity of each spectrum was calculated and analyzed with the Fourier transform. A distribution with a slight increase of 30% was observed around 3.3 Hz; this could be the mechanical eigenfrequency of the telescope. The increase was compensated for by a damping filter. The relative slope of the intensity was calculated and observed in a histogram—the very sudden changes caused by passing birds could easily be detected by employing a threshold. Several smaller events could be detected by lowering the threshold, but a refined analysis of the spectra from these events is not meaningful due to the close-lying noise levels. In the time frame of these measurements, we detected 16 rather large events. Typically, each event was resolved by two to four spectra, recorded with a time separation of 0.02 s. Most events, except for the one presented in Fig. 12, showed up as sudden drops in the static
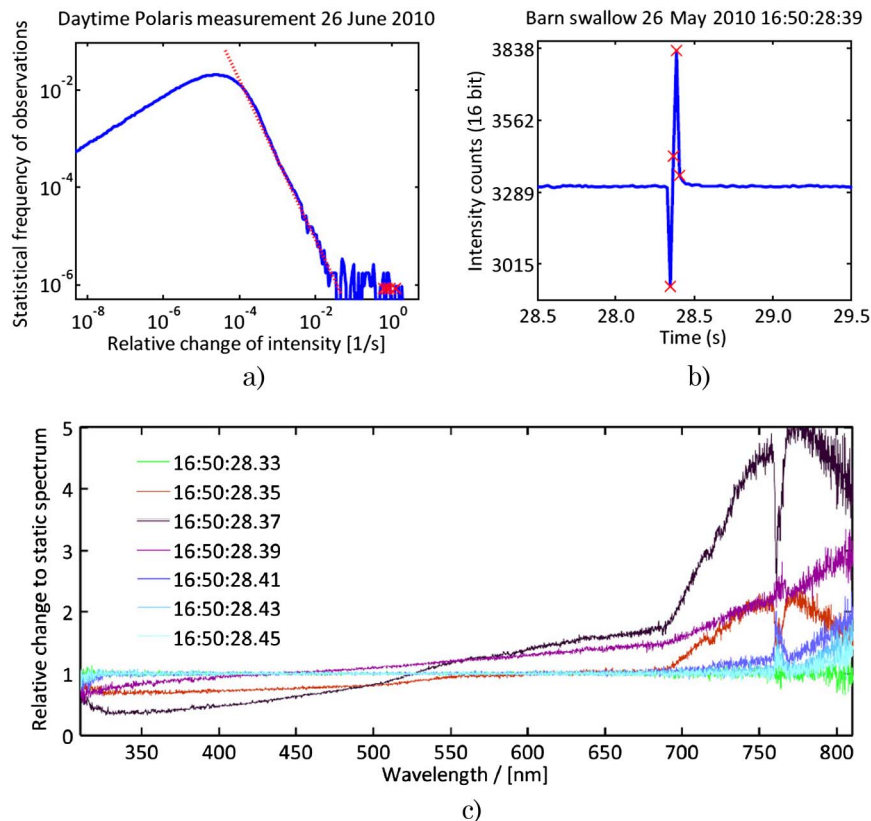
Fig. 12. (Color online) a) Histogram of relative slopes in total intensity enables us to determine a threshold for rare events. Crosses mark the events detected in Fig. 12b). b) Change in total collected mean intensity when a barn swallow passes by at 12:49 on 26 May 2010. c) Spectral intensity change relative to the static sky spectrum during the same event as in b).

intensity, resulting from an obscuration of the "sky" radiation. When analyzed in the spectral domain, the events were normalized with the quasi-static spectra at the time of the event. Most event spectra showed a flat ratio in the UV and VIS from 350 to 700 nm. Two of the events showed an intensity rise at around 550 nm. Both of these events arose from barn swallows passing roughly 30 m over the telescope, and thus features are presumed to be associated with their red pheomelanized throat. The events occurring at clear sky show an increase in the NIR just after 700 nm. This is interpreted as the vegetation-covered ground illuminating the birds from below (vegetation reflection is known to dramatically increase above 700 nm [57]). The increase in the NIR did not apply to the oxygen A band around 760 nm, a terrestrial Fraunhofer line of much interest in remote sensing of Sun-induced vegetation fluorescence (see, e.g., [58]). In a few spectra, the intensity in the 760 nm band was larger than in the remaining IR spectra; this could be caused by direct reflection of the sunlight in the bird, with the implication that the path length Sun–bird–telescope is smaller than the mean Sun–atmosphere–telescope path length when looking toward Polaris. Although no species-specific information can be expected in the NIR due to the lack of spectral bands in bird vision and therefore also chromophores in the plumage, reflectance of ground vegetation and information from Fraunhofer

lines, such as the oxygen band around 760 nm, could provide clues on the geometry of the event, altitude, and surface orientation. A better understanding of this would, however, require a larger sample number and altitude span of the recorded flying birds.

Although we applied a similar analysis to the data obtained by moon tracking where samples with the highest slopes were investigated, we unfortunately did not find any significant events there.

4. Discussion, Conclusions, and Perspectives

The isosurface histogram exemplified in Fig. 5 was obtained with the multi-PMT setup on museum birds with the wings kept along the sides. In a live situation, a single shot would illuminate the bird in some part of its wing cycle, and the result might vary accordingly. The dependence on wing-beat phase could provide an additional source of information for species with varying pigmentation over the body, including the underwing coverts and primaries, where we could expect some sort of "doughnut" trajectory to arise in the color space. This fact could be exploited in the same way as proposed for the IR imaging, utilizing a tracking system. In a realistic situation, detection of the IR signal could be achieved by separating MIR light from the lidar telescope into the two bands using a dichroic beam splitter. Making one of these a quadrant detector would allow for bird tracking by feeding the differential signals of opposite

quadrants back to the motors controlling the elevation and horizontal angle of the folding mirror. If no opportunity for tracking is forthcoming, the information from the IR detection could still allow for indexing the lidar hit with regard to the phase of the wing cycle.

In our case, we present a color space with the normalized contributions to each spectral band. In principle, with profound calibration, the space could be linearly transformed into a concentration space with, e.g., eumelanin, pheomelanin, and lutein absorbance on the axes.

It should be noted that during lidar measurements, a large divergence of the beam will increase the probability of illuminating a bird, but, at the same time, the amount of light in each hit, and thus the signal-to-noise ratio, will unavoidably also decrease. The divergence has, therefore, to be decided depending on the current conditions. If tracking is employed, the divergence could be kept small.

Laboratory reflectance studies show that the reflectance at 266 nm is low and dominated by the specular reflection. It is also clear that the reflectance does not vary much between species, and we can conclude that the exact value is unstable and depends heavily on geometry effects, such as illumination angle. This tells us that the depolarized signal is preferred for normalization due to its better stability and independence of such effects. These results also go well in hand with the remote depolarization measurements performed with the lidar. The results from these show an insignificant difference between species, and as an example, the black rook and the herring gull, completely different in terms of abundance of chromophores, show similar DPRs. From this we can conclude that the DPR at 266 nm is probably not a good candidate for classification, but also that the excitation quenching by chromophores is insignificant at a wavelength of 266 nm. The larger differences of reflectance between the birds at longer wavelengths could possibly be utilized for species-dependent DPRs there.

The gray heron is a wetland bird feeding on fish and amphibians by frozen posture hiding at water edges and slow walking through the water in lakes and rivers. The male gray heron, as many other heron species, carries longer feathers on the back and breast, which are used in displays during the mating season. It is likely that the reflection characteristics of these feathers on the breast have evolved as an adaptation to foraging (camouflage) or mate choice, which in the latter case has been shown for several other bird species, including, e.g., the blue tit [59]. This could be one explanation to the high-UV reflectance observed for this bird.

The measurements of wing cycle dependence of the IR signals have been limited to single feathers, and a simplified wing model has been applied, where the wing feathers are aligned parallel to the air flow. Extrapolation to a more realistic situation is not trivial. However, symmetry around 0° incidence in the band ratio implies that the total signal from feathers (wings) with opposite orientations will aggregate rather than average out. Further, the highly inelastic MIR–photon migration through plumage could potentially enhance structural features in the outermost layers. It should be noted, that apart from the spectral changes, wing beating will also contribute to a prominent (and trivial) intensity modulation as the wing cross section observed from ground level varies.

Three IR transmittance spectra at normal incidence are presented, which represent natural spectral fingerprints that may be shared by a number of birds. The general shape of the spectra is defined by the β-keratin absorption profile, which is essentially identical for all feathers, with the angular-dependent interference profile superimposed, whose central maximum at normal incidence, and the angular dependence of the same is dependent on bird species. As mentioned previously, this is likely due to the geometry of the barbules, and possibly the inclination of these with regard to the feather surface. The surface normal defining the plane of this effective optical surface of the feather may be determined, e.g., using reflectance measurements by scanning the angle in two axes and finding the maximum reflected intensity; our current equipment does not allow this. Full classification based on MIR spectral data alone is not realistic, because several birds may exhibit similar spectral fingerprints, but in the context of LIF lidar providing chemical information, the additional MIR information gained on the microstructure compliments LIF in a natural way. Because the effects thus incorporated have a wide spectral origin, from deep UV to MIR, they are likely to be the result of different physical phenomena, which indicates a large classification possibility. Reflectance measurements with active transmitters in the MIR would be an obvious complement to the transmittance spectra. Further, polarization analysis may shed more light on the cause of the interference effects.

The ability to perform remote IR analysis of live birds will likely depend on the degree to which the order of the feather structure is maintained in the plumage, as opposed to in single feathers. In contrast to VIS iridescent colors, the photon transport in the deeper lying plumage can be expected to be highly inelastic and could reinforce the structural signatures. Absolute wing-beat phase information is accurately predicted from the theoretical peak transmittance wavelength waveform, which provides important information for the LIF measurements in order to aid determination of which part of the bird that is being sampled.

The passive scattering studies correspond to a minimal portable setup, requiring only a telescope, a compact spectrometer and a laptop, thus making it ideal as a standalone method. However, similar signals could be retrieved for free in a lidar setup [31]. We have proposed a feasible method for instrument calibration and rare event detection based on the

relative slope of intensity change, and demonstrated spectral features associated with atmospheric path length and gases, subillumination from vegetation, and embedded chromophores on the birds. More statistics and larger altitude span are needed to draw conclusions regarding the Fraunhofer lines and the possibility for altitude determination of the passing birds.

Our findings imply three new feasible methods for remote classification of night-migrating and high-altitude flying birds. To date, little is known about the migration ecology of specific night-migrating species due to that current techniques do not allow species level identification, apart from a few exceptions. Applying the techniques described above could add information that enables biologists to identify some species and thus to address an entirely new set of questions for studies of the migration and flight adaptations of these species. Important insights in timing of migration, flight directions in relation to winds and topography, as well as monitoring of passing species could be accomplished. Such information is crucial for understanding basic biology, such as how wing morphology affects flight patterns during migration. Questions of more general interest, such as where and when different species that are hosts to diseases such as avian flu and tick-borne diseases are migrating, could also be resolved using such information [3,4,9]. Further development of these techniques to be more practically applicable in field situations could be a fruitful approach for exciting advantages in bird migration research.

References

1. S. Åkesson and A. Hedenström, "How migrants get there: migratory performance and orientation," BioScience **57**, 123–133 (2007).
2. T. Alerstam and Å. Lindström, "Optimal bird migration: the relative importance of time, energy and safety," in *Bird Migration: Physiology and Ecophysiology*, E. Gewinner, ed. (Springer-Verlag, 1990), pp. 331–351.
3. T. Alerstam, A. Hedenström, and S. Åkesson, "Long-distance migration: evolution and determinants," Oikos **103**, 247–260 (2003).
4. B. Bruderer and F. Liechti, "Intensität, Höhe und Richtung von Tag- und Nachtzug im Herbst über Südwestdeutschland," Ornithol. Beob. **95**, 113–128 (1998).
5. S. Zehnder, S. Åkesson, F. Liechti, and B. Bruderer, "Nocturnal autumn bird migration at Falsterbo, south Sweden," J. Avian Biol. **32**, 239–248 (2001).
6. P. Kerlinger and F. R. Moore, *Atmospheric Structure and Avian Migration* (Plenum, 1989).
7. Å. Lindström, "The role of predation risk in stopover habitat selection in migrating bramblings, *Fringilla montifringilla*," Behav. Ecol. **1**, 24–35 (1990).
8. P. Henningsson, G. Spedding, and A. Hedenstrom, "Vortex wake and flight kinematics of a swift in cruising flight in a wind tunnel," J. Exp. Biol. **211**, 717–730 (2008).
9. I. Newton, *The Migration Ecology of Birds* (Academic, 2008).
10. D. W. H. Adams, "Radar observations of bird migration in Cyprus," Ibis **104**, 133–146 (1962).
11. T. Alerstam, "Nocturnal migration of thrushes (*Turdus* spp.) in southern Sweden," Oikos **27**, 457–475 (1976).
12. T. Alerstam, J. Bäckman, G. A. Gudmundsson, A. Hedenström, S. S. Henningsson, H. Karlsson, M. Rosén, and R. Strandberg, "A polar system of intercontinental bird migration," Proc. R. Soc. B **274**, 2523–2530 (2007).
13. M. B. Casement, "Migration across the Mediterranean observed by radar," Ibis **108**, 461–491 (1966).
14. J. L. F. Parslow, "The migration of passerine night migrants across the English Channel studied by radar," Ibis **111**, 48–79 (1969).
15. B. Bruderer and F. Liechti, "Quantification of bird migration—different means compared," in *Proceedings of the Bird Strike Committee, Europe*, Vol. 22 (Bird Strike Committee Europe, 1994), pp. 243–254.
16. S. Åkesson, "Coastal migration and wind drift compensation in nocturnal passerine migrants," Ornis Scand. **24**, 87–94 (1993).
17. S. A. Gauthreaux, Jr., "A portable ceilometer technique for studying low level nocturnal migration," Bird Banding **40**, 309–320 (1969).
18. F. Liechti, "Calibrating the moon-watching method—changes and limits," Avian Ecol. Beh. **7**, 27–41 (2001).
19. F. Liechti, D. Peter, R. Lardelli, and B. Bruderer, "Herbstlicher Vogelzug im Alpenraum nach Mond-beobachtungen—Topographie un Wind beeinflussen den Zugverlauf," Ornithol. Beob. **93**, 131–152 (1996).
20. S. A. Gauthreaux and J. W. Livingston, "Monitoring bird migration with a fixed-beam radar and a thermal-imaging camera," J. Field Ornithol. **77**, 319–328 (2006).
21. F. Liechti, B. Bruderer, and H. Paproth, "Quantification of nocturnal bird migration by moonwatching: comparison with radar and infrared observations," J. Field Ornithol. **66**, 457–468 (1995).
22. A. Farnsworth, S. A. Gauthreaux, Jr., and D. van Blaricom, "A comparison of nocturnal call counts of migrating birds and reflectivity measurements on Doppler radar," J. Avian Biol. **35**, 365–369 (2004).
23. A. Farnsworth and I. J. Lovette, "Evolution of nocturnal flight calls in migrating wood-warblers: apparent lack of morphological constraints," J. Avian Biol. **36**, 337–347 (2005).
24. B. J. Stutchbury, S. A. Tarof, T. Done, E. Gow, P. M. Kramer, J. Tautin, J. W. Fox, and V. Afanasyev, "Tracking long-distance songbird migration by using geolocators," Science **323**, 896–896 (2009).
25. J. Meade, D. Biro, and T. Guilford, "Homing pigeons develop local route stereotypy," Proc. R. Soc. B **272**, 17–23 (2005).

26. T. Alerstam, M. Rosén, J. Bäckman, P. G. Ericson, and O. Hellgren, "Flight speeds among bird species: allometric and phylogenetic effects," PLos Biol. **5**, 1656–1662 (2007).

27. J. Bäckman and T. Alerstam, "Confronting the winds: orientation and flight behaviour of roosting swifts, *Apus apus*," Proc. R. Soc. B **268**, 1081–1087 (2001).

28. B. Bruderer and E. Weitnauer, "Radarbeobachtungen über Zug und Nachtflüge des Mauerseglers (*Apus Apus*)," Rev. Suisse Zool. **79**, 1190–1200 (1972).

29. G. E. Hill and K. J. McGraw, *Bird Coloration, Mechanisms and Measurements*, Vol. 1 (Harvard University Press, 2006).

30. H. Noh, S. F. Liew, V. Saranathan, S. G. J. Mochrie, R. O. Prum, E. R. Dufresne, and H. Cao, "How noniridescent colors are generated by quasi-ordered structures of bird feathers," Adv. Mat. **22**, 2871–288 (2010).

31. M. Brydegaard, P. Lundin, Z. G. Guan, A. Runemark, S. Åkesson, and S. Svanberg, "Feasibility study: fluorescence lidar for remote bird classification," Appl. Opt. **49**, 4531–4544 (2010).

32. M. A. Mycek and B. W. Pogue, eds., *Handbook of Biomedical Fluorescence* (CRC Press, 2003).

33. N. Takeuchi, "Elastic lidar measurement of the troposphere," in *Laser Remote Sensing*, T. Fujii and T. Fukuchi, eds. (CRC Press, 2005), pp. 63–122.

34. C. M. R. Platt, J. C. Scott, and A. C. Dilley, "Remote sounding of high clouds. part VI: optical properties of mid-latitude and tropical cirrus," J. Atmos. Sci. **44**, 729–747 (1987).

35. R. G. Strauch, V. E. Derr, and R. E. Cupp, "Atmospheric temperature measurement using Raman backscatter," Appl. Opt. **10**, 2665–2669 (1971).

36. G. Benedetti-Michelangeli, F. Gongeduti, and G. Fiocco, "Measurement of aerosol motion and wind velocity in the lower troposphere by Doppler optical radar," J. Atmos. Sci. **29**, 906–910 (1972).

37. R. Grönlund, M. Sjöholm, P. Weibring, H. Edner, and S. Svanberg, "Elemental mercury emissions from chlor-alkali plants measured by lidar techniques," Atmos. Environ. **39**, 7474–7480 (2005).

38. N. Menyuk, D. K. Killinger, and W. E. DeFeo, "Remote sensing of NO using a differential lidar," Appl. Opt. **19**, 3282–3286 (1980).

39. Z. G. Guan, P. Lundin, L. Mei, G. Somesfalean, and S. Svanberg, "Vertical lidar sounding of atomic mercury and nitric oxide in a major Chinese city," Appl. Phys. B **101**, 465–470 (2010).

40. J. Gelbwachs and M. Birnbaum, "Fluorescence of atmospheric aerosols and lidar implications," Appl. Opt. **12**, 2442–2447 (1973).

41. P. Weibring, T. Johansson, H. Edner, S. Svanberg, B. Sundnér, V. Raimondi, G. Cecchi, and L. Pantani, "Fluorescence lidar imaging of historical monuments," Appl. Opt. **40**, 6111–6120 (2001).

42. A. Ounis, Z. G. Cerovic, J. M. Briantais, and I. Moya, "DE-FLIDAR: a new remote sensing instrument for estimation of epidermal UV absorption in leaves and canopies," in *Proceedings of the European Association of Remote Sensing Laboratories (EARSeL)-SIGWorkshop LIDAR*, Vol. 1 (EARSeL, 2000), pp. 196–204.

43. S. Svanberg, "LIDAR," in *Springer Handbook of Lasers and Optics*, F. Träger, ed. (Springer-Verlag, 2007), pp. 1031–1052.

44. T. Fujii and T. Fukuchi, eds., *Laser Remote Sensing* (CRC Press, 2005).

45. R. B. Bradbury, R. A. Hill, D. C. Mason, S. A. Hinsley, J. D. Wilson, H. Balzter, G. Q. A. Anderson, M. J. Whittingham, I. J. Davenport, and P. E. Bellamy, "Modelling relationships between birds and vegetation structure using airborne lidar data: a review with case studies from agricultural and woodland environments," Ibis **147**, 443–452 (2005).

46. R. Clawges, K. Vierling, L. Vierling, and E. Rowell, "The use of airborne lidar to assess avian species diversity, density, and occurrence in a pine/aspen forest," Remote Sens. Environ. **112**, 2064–2073 (2008).

47. N. E. Seavy, J. H. Viers, and J. K. Wood, "Riparian bird response to vegetation structure: a multiscale analysis using lidar measurements of canopy height," Ecol. Appl. **19**, 1848–1857 (2009).

48. P. Weibring, H. Edner, and S. Svanberg, "Versatile mobile lidar system for environmental monitoring," Appl. Opt. **42**, 3583–3594 (2003).

49. R. O. Prum, "Anatomy, physics and evolution of structural colors," in *Bird Coloration, Mechanisms and Measurements*, G. E. Hill and K. J. McGraw, eds., Vol. 1 (Harvard University Press, 2006), pp. 295–354.

50. M. Srinivasarau, "Nano-optics in the biological world," Chem. Rev. **99**, 1935–1961 (1999).

51. C. Giacovazzo, H. L. Monaco, G. Artioli, D. Viterbo, G. Ferraris, G. Gilli, G. Zanotti, and M. Catti, *Fundamentals of Crystallography* (Oxford University Press, 2002).

52. N. S. Hart, J. C. Partridge, and I. C. Cuthill, "Visual pigments, cone oil droplets and cone photoreceptor distribution in the European starling (*Sturnus vulgaris*)," J. Exp. Biol. **201**, 1433–1446 (1998).

53. Z. G. Guan, M. Brydegaard, P. Lundin, M. Wellenreuther, A. Runemark, E. I. Svensson, and S. Svanberg, "Insect monitoring with fluorescence lidar techniques: field experiments," Appl. Opt. **49**, 5133–5142 (2010).

54. C.V. Raman, "The theory of the Christiansen experiment," Proc. Indian Acad. Sci. **A29**, 381–390 (1949).

55. G. B. Benedek, "Theory of transparency of the eye," Appl. Opt. **10**, 459–473 (1971).

56. R. O. Prum and R. H. Torres, "A Fourier tool for the analysis of coherent light scattering by bio-optical nanostructures," Integr. Comp. Biol. **43**, 591–602 (2003).

57. S. Svanberg, *Atomic and Molecular Spectroscopy—Basic Aspects and Practical Applications*, 4th ed. (Springer-Verlag, 2004).

58. U. Rascher, B. Gioli, and F. Miglietta, "FLEX—fluorescence explorer: a remote sensing approach to quantify spatio-temporal variations of photosynthetic efficiency from space," Photosynth. Res. **91**, 293–294 (2007).

59. S. Hunt, A. T. Bennett, I. C. Cuthill, and R. Griffiths, "Blue tits are ultraviolet tits," Proc. R. Soc. Lond. B **265**, 451–455 (1998).